

The effect of liquid nitriding on the corrosion resistance of AISI 304 austenitic stainless steel in H₂S environments

Li, Longyi; Wang, Jun ; Yan, Jing; Duan, Liang; Li, Xiaoying; Dong, Hanshan

DOI:

[10.1007/s11661-018-4920-9](https://doi.org/10.1007/s11661-018-4920-9)

License:

Other (please specify with Rights Statement)

Document Version

Peer reviewed version

Citation for published version (Harvard):

Li, L, Wang, J, Yan, J, Duan, L, Li, X & Dong, H 2018, 'The effect of liquid nitriding on the corrosion resistance of AISI 304 austenitic stainless steel in H₂S environments', *Metallurgical and Materials Transactions A: Physical Metallurgy and Materials Science*. <https://doi.org/10.1007/s11661-018-4920-9>

[Link to publication on Research at Birmingham portal](#)

Publisher Rights Statement:

This is a post-peer-review, pre-copyedit version of an article published in Metallurgical and Materials Transactions A. The final authenticated version is available online at: <http://dx.doi.org/10.1007/s11661-018-4920-9>

General rights

Unless a licence is specified above, all rights (including copyright and moral rights) in this document are retained by the authors and/or the copyright holders. The express permission of the copyright holder must be obtained for any use of this material other than for purposes permitted by law.

- Users may freely distribute the URL that is used to identify this publication.
- Users may download and/or print one copy of the publication from the University of Birmingham research portal for the purpose of private study or non-commercial research.
- User may use extracts from the document in line with the concept of 'fair dealing' under the Copyright, Designs and Patents Act 1988 (?)
- Users may not further distribute the material nor use it for the purposes of commercial gain.

Where a licence is displayed above, please note the terms and conditions of the licence govern your use of this document.

When citing, please reference the published version.

Take down policy

While the University of Birmingham exercises care and attention in making items available there are rare occasions when an item has been uploaded in error or has been deemed to be commercially or otherwise sensitive.

If you believe that this is the case for this document, please contact UBIRA@lists.bham.ac.uk providing details and we will remove access to the work immediately and investigate.

The effect of liquid nitriding on the corrosion resistance of AISI 304 austenitic stainless steel in H₂S environments

Longyi Li ^a, Jun Wang ^{a*}, Jing Yan ^b, Lian Duan ^a, Xiaoying Li ^c, Hanshan Dong ^c

^a College of Manufacturing Science and Engineering, Sichuan University, 610065, Chengdu, PR China

^b Research Institute of Natural Gas Technology, PetroChina Southwest Oil and Gas Field Company, 610213, Chengdu, PR China.

^c School of Metallurgy and Materials, University of Birmingham, Edgbaston, Birmingham B15 2TT, UK

Abstract: AISI 304 austenitic stainless steel was low-temperature liquid nitrided in a molten salt bath at 703 K for 8 h, which produced a 3-layered structure consisting of a top oxide layer, an intermediate nitrogen-rich layer and a bottom carbon-rich layer. The effect of nitriding on its corrosion resistance was investigated in a H₂S environment. The corrosion rate of the untreated sample is about 3.3 times that of the nitrided sample after H₂S corrosion. Corrosion pits can be clearly observed on the surface of the untreated sample, while the nitrided sample surface remained relatively intact. Both the oxide layer and the nitrogen-rich layer can help reduce the hydrogen permeation, which is beneficial for combating hydrogen embrittlement. The corrosion products mainly consisted of oxides, hydroxides, and sulfates. The nitrided layers can serve as a barrier to corrosion, thus preventing the corrosion of the substrate material. Active nitrogen in the nitrided layer reacts with H⁺ ions to form NH₄⁺, which effectively prevents further acidification of the local area and inhibits the occurrence of pitting corrosion and the dissolution rate of the metal in the etching hole, thus improving the local corrosion resistance of the stainless steel.

Key words: austenite stainless steels, expand austenite, corrosion resistance, liquid nitriding, surface treatment

1. Introduction

Austenite stainless steel is widely used in various industrial fields due to its excellent corrosion resistance and mechanical properties. With the increasing exploitation and processing of high sulfur oil and gas field, H₂S corrosion has become a widespread concern.^[1] H₂S is one of the most dangerous factors causing metal corrosion in acidic oil and gas environments, and electrochemical corrosion will occur on the surface of the pipeline used.^[2] In recent years, many researchers have conducted extensive research on the local corrosion and stress corrosion cracking (SCC) mechanism of stainless steel in H₂S medium. The research was focused on the

* Corresponding author. E-mail address: Srwangjun@scu.edu.cn (J. Wang)

40 structure, properties, formation process and external factors of corrosion products in
41 saturated H₂S systems.^[3-6] Ding et al. investigated the behavior of corrosion and SCC
42 of austenitic stainless steels in high H₂S–CO₂–Cl⁻ environments. ^[7] Their results
43 showed that high H₂S–CO₂ pressure can accelerate anodic dissolution process,
44 deteriorate passive films, and aggravate SCC sensitivity. The corrosion rate of steel in
45 wet H₂S is significantly higher than that in dry H₂S environment.^[8] H₂S reacted with
46 metals to form surface metal sulfides, and released hydrogen atoms, which were
47 absorbed by the metal surface and caused hydrogen embrittlement.^[9] Besides, low pH
48 can promote both cathodic and anodic actions on stainless steel and facilitate passive
49 film breakdown.^[7]

50 In addition to the corrosion of H₂S, CO₂ and Cl⁻, saturated natural gas in
51 pipelines will have a free liquid phase due to the effect of pressure drop, and a certain
52 amount of solid impurities will be mixed in the pipeline, resulting in three-phase
53 coexistence of gas, solid, and liquid. Erosion-corrosion is faster than corrosion alone
54 and is a more hazardous local corrosion.^[10] When corrosive liquid contains solid
55 particles (such as insoluble salts, sand, drilling fluid, etc.), it is more likely to cause
56 such erosion-corrosion damage. Austenitic stainless steels have a low carbon content
57 (mass fraction below 0.03 %), resulting in a low surface hardness and poor wear
58 resistance. The service life of stainless steel pipes under such conditions will be
59 seriously reduced, and so it is necessary to improve their surface hardness and
60 strength on the premise of ensuring its good comprehensive performance.

61 It has been reported previously that austenitic stainless steels are
62 thermochemically treated (carburized or nitrided) at low temperatures to form
63 interstitial atoms supersaturated non-deposition layers. ^[11-12] After the treatment, a
64 layer with a high concentration of nitrogen and/or carbon will be formed on the
65 surface of the treated austenitic stainless steel. This surface layer can effectively
66 improve the hardness, wear resistance, fatigue resistance and corrosion resistance of
67 the material, which is so-called S-phase or expanded austenite.^[12] Low-temperature
68 nitriding has been shown to significantly improve pitting potential. Dong discovered
69 that low temperature nitrided 316 stainless steel showed excellent resistance to pitting
70 of chlorine containing solution, and the increased corrosion resistance of the nitride S
71 phase layer is thought to be due to its high nitrogen content.^[13] The enhancement in
72 corrosion resistance of austenitic stainless steels by nitriding or carbonization
73 treatment may be related to a high surface interstitial atom concentration or a large
74 surface residual compressive stress due to interstitial atoms.^[14]

75 Zhang et al. performed Quench-Polish-Quench (QPQ) salt bath compound
76 treatment on GX-8 alloy steel and found that the dense oxide film Fe₃O₄ could
77 significantly reduce the friction coefficient of the material at 573 K, and the corrosion
78 resistance of the material was greatly improved before the oxide film was ruptured.^[15]
79 However, the QPQ treatment is a multi-step and hence relatively complicated process.
80 In contrast, low-temperature salt bath nitriding does not require an additional
81 oxidation process to form a surface oxide layer. Hence, the salt bath nitriding process
82 is simpler and the cost of the equipment is lower than the QPQ process.

83 The aim of the present paper was to study the effect of low-temperature liquid

84 bath nitriding on the corrosion resistance of AISI 304 austenitic stainless steel in a
85 H₂S containing environment. Through the H₂S immersion corrosion tests, the
86 corrosion behavior and the corrosion mechanism of low temperature salt bath nitride
87 304 austenitic stainless steel in H₂S containing environments (such as pipelines for oil
88 and gas applications) were studied. The low-temperature nitriding is expected to be
89 applied to the pipelines used for oil-gas fields, significantly extending their service
90 life in the H₂S corrosion environment.

92 2. Experimental

93 2.1 Material

94 The material used in this experiment was cast 304 stainless steel, taken from the
95 natural gas valve castings supplied by Southwest Natural Gas Research Institute ,
96 China. The chemical composition provided by the materials supplier is shown in
97 Table 1. The samples were ground with abrasive papers from 400# down to 1200#,
98 degreased with a mixture of 50 vol% ethanol and 50 vol% acetone, and finally
99 washed with deionized water and dried in atmosphere.

100
101 **Table 1** Chemical composition of AISI 304 stainless steel (mass%)

Element	C	Cr	Ni	Mn	Si	S	P	Fe
Pct	0.035	18.640	8.010	1.100	0.436	0.020	0.013	Balance

102 2.2 Liquid bath nitriding and H₂S corrosion test

103 The chemicals used in this experiment for liquid bath nitriding were non-toxic
104 cyanate, chloride and carbonate salts. The nitriding process involved immersing the
105 sample in 703 K molten salt for 8 hours, during which the non-toxic cyanate
106 decomposes into carbon atoms and nitrogen atoms, forming a high chemical potential
107 on the surface of the samples. More details can be found in literature.^[16] This high
108 chemical potential promotes the diffusion of the nitrogen and carbon atoms into the
109 austenitic stainless steel sample, thus forming a large supersaturation of N(C) in its
110 surface.

111 H₂S corrosion tests were conducted in accordance with NACE TM0177-2005
112 standard using the solution ‘A’ recommended by NACE TM0177-2005. Both the
113 untreated and nitrated samples were soaked in this solution for 720 hours.

114 Before the H₂S corrosion test, the mass of the sample (m) was weighed and
115 recorded. At the end of the test, the corroded sample was taken out, and the corrosion
116 product formed on the surface was removed with an acid stripping solution (500 ml
117 HCl + 500 ml H₂O + 3.5 g C₆H₁₂N₄). The sample was degreased with acetone and
118 then dried in a box. After drying for 24 hours, the sample was taken out for weighing
119 (m_t), and the corrosion rate was calculated based on the weight loss during the test.
120 The uniform corrosion rate (R_{corr}) is calculated as follows:
121 $R_{corr}=8.76\times 10^4\times(m-m_t)/(S_1\times\rho\times t)$, where S₁ is the total area of the test piece (32 cm²);
122 ρ is the density of the test piece material (7.9 g/cm³); and t is the test time (720 h).

123 2.3 Hydrogen permeation test

124 Hydrogen permeation testing was performed in line with ASTM G148 standard
125 using a type Avanathan-Stachursky double-electrolytic cell produced by Wuhan
126 Corrtest, China.^[17] Three sets of samples were prepared: untreated samples,
127 as-nitrided samples and the nitride samples whose surface oxide film was removed by
128 mechanical polishing. The samples used in this test were stainless steel wafer
129 electrodes with a working surface of 1.77 cm² and a thickness of 0.2 mm. The
130 experimental conditions were decided by referring to literature.^[18-19] The experimental
131 solution is 0.5 mol/L sulfuric acid with 1 g/L CH₄N₂S, and the hydrogen charge
132 current is 20 mA/cm² with an anode potential of 300 mV. Before the test solution was
133 added, the sample was passivated in a 0.2 mol/L NaOH solution for more than 24 h, in
134 order that the background current density is less than 0.1 μA/cm².^[20]

135 The hydrogen diffusion flux (J_{∞}) is calculated from the anode steady-state current
136 (I_{∞}) and can be expressed as:

$$137 J_{\infty} = \frac{I_{\infty}}{A} \quad [21]$$

138 Where: A is the area of the sample in contact with the solution; F is the Faraday
139 constant.

140 The effective hydrogen diffusion coefficient (D_{eff}) can be calculated using the formula
141 below:

$$142 D_{\text{eff}} = \frac{J_{\infty}^2}{I_{\text{a}}^2} \quad [22]$$

143 Where: t is the thickness of the sample; t_L is the delay time. The delay time is
144 approximately equal to the time taken for the hydrogen charging current density to
145 reach 0.63 times the steady-state anode current density, i.e. the time used for
146 $I_{\text{a}} = 0.63I_{\infty}$. The hydrogen concentration C_0 at the hydrogen end can be estimated by
147 the following formula:

$$148 C_0 = \frac{J_{\infty}^2}{D_{\text{eff}}} \quad [22]$$

149 2.4 Microstructural characterization

150 The cross section of the sample before and after the H₂S corrosion tests was
151 mechanically polished and chemically etched with an etchant formulated with 50
152 vol% HCl, 25 vol% HNO₃, and 25 vol% H₂O. The OLYMPUS GX51 optical
153 microscope and JSM-7500F scanning electron microscope were used for
154 microstructural analysis. The surface phases were studied using the EMPYREAN
155 X-ray diffractometer (XRD) with a scanning range of 20 to 110 degrees with Cu K α
156 radiation ($\lambda = 0.15418\text{nm}$). The SHIMADZU-1720 electron probe microanalyzer
157 (EPMA) was used to quantitatively analyze the elemental distribution from the
158 surface to the matrix. X-ray photoelectron spectroscopy (XPS) was used to analyze
159 the surface corrosion products.

160 3. Results

161 3.1 Characteristics of the nitrided layers

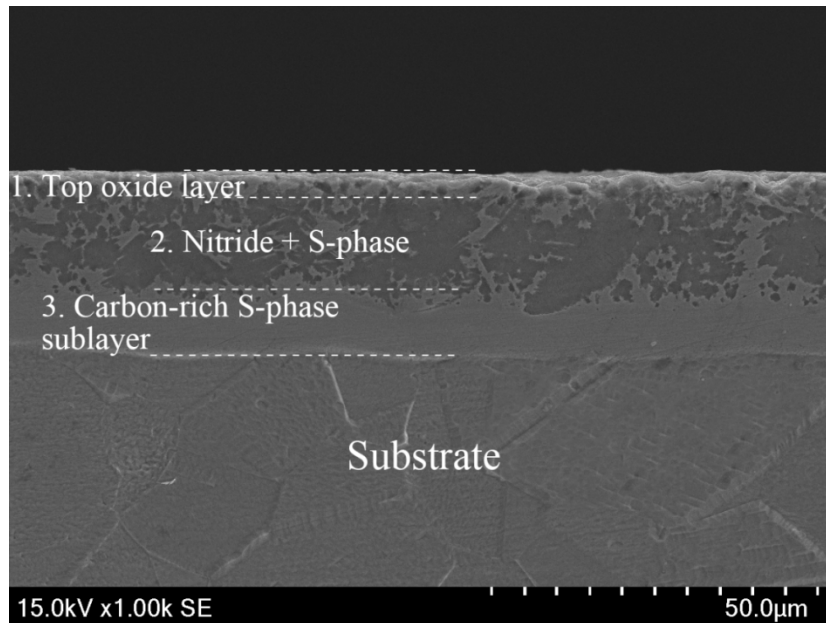


Fig.1 A typical cross sectional SEM image of nitrided sample

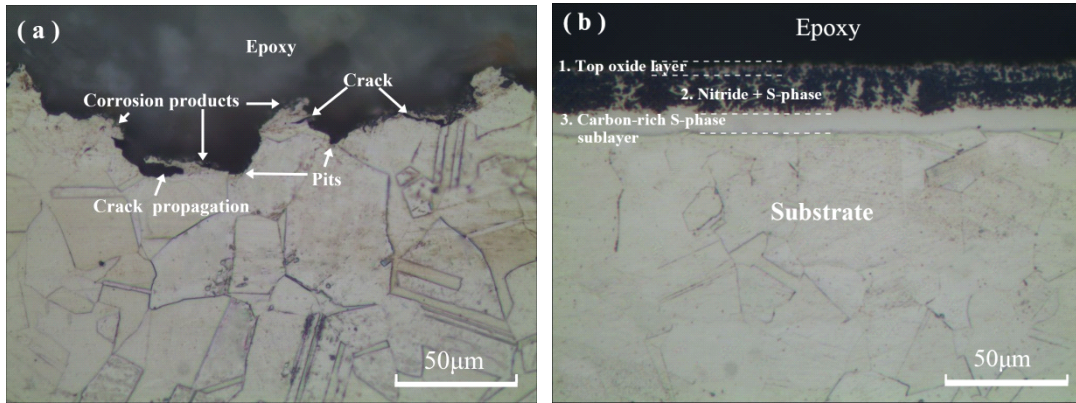
162
163
164

165 Figure 1 shows the cross-sectional photomicrograph of the AISI304 austenitic
166 stainless steel after low-temperature salt bath nitriding treatment. The substrate shows
167 clear grain boundaries after etching with the etchant. The salt bath nitriding produced
168 a 3-layered structure consisting of an oxide top layer, followed by a nitrogen-rich
169 layer and a carbon-rich layer. The atomic nitrogen was formed from the following
170 CNO^- dissociation reaction: $4\text{CNO}^- \rightarrow 2\text{CN}^- + \text{CO}_3^{2-} + \text{CO} + [\text{N}]$. Carburizing is also
171 promoted by the liberation of atomic carbon species according to the following CO
172 dissociation reaction: $\text{CO} \rightarrow \text{CO}_2 + [\text{C}]$. Under the same treatment conditions, the
173 thickness of the nitrided layer is larger than that of the carburized layer. This is mainly
174 due to the fact that the atomic radius of N is smaller than that of the C atom, and the
175 energy required for N atoms to enter the lattice is smaller than that for C atoms. Under
176 the same conditions, the nitrogen atoms can diffuse deeper than carbon atoms.
177 Tsujikawa et al. used simultaneous carburizing and nitriding process to obtain a
178 similar layer on the surface of austenitic stainless steel.^[23] Due to the long processing
179 time, certain Cr nitrides appear in the nitrided layer.

180 3.2 Corrosion morphology and corrosion rate

181 Nitrided samples and as-received 304 samples were immersed in H_2S solution
182 for 720 h and the cross-sectional micrographs are shown in the Figure 2.

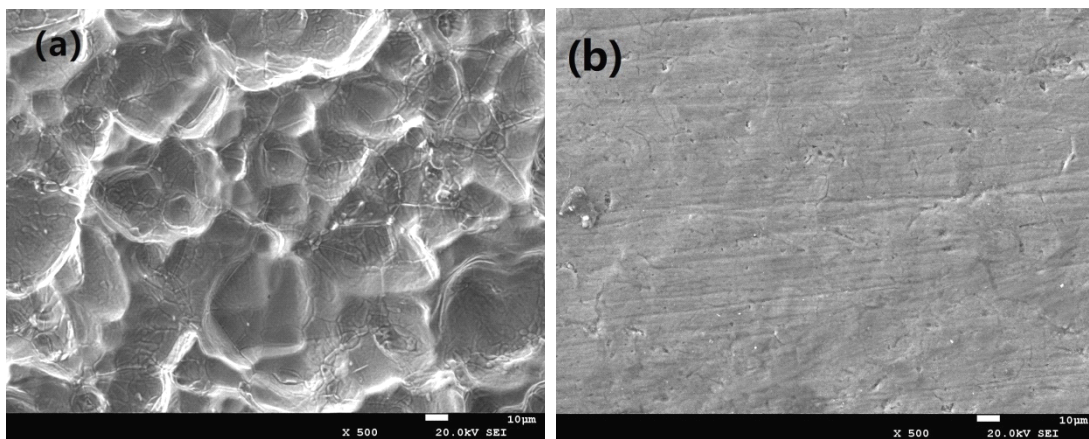
183 As shown in Figure 2(a), a number of pits and cracks were observed from the
184 cross-section of the untreated sample, which indicates pitting and cracking of the
185 sample. In the process of crack propagation, the width and depth of the crack
186 continuously increased, and the outer layer material eventually spalled off. In contrast,
187 neither pits nor cracks were observed from the cross-section of the nitrided samples
188 after H_2S corrosion test (Fig.2(b)).



189

190 **Fig.2** Cross-sectional optical micrographs (OM): (a) untreated sample (b) nitrided sample after
 191 immersion in H₂S solution for 720h

192 Figure 3 shows the surface morphology of the untreated and nitrided samples after
 193 immersion in H₂S solution for 720h. Many agglomerates were formed on the surface
 194 of the untreated sample (Fig.3(a)), which is generally considered to be corrosion
 195 product FeS. The surface of the nitrided sample remained intact as evidenced by the
 196 existence of the original grinding marks with almost no corrosion product (Fig.3(b)).



197

198 **Fig.3** SEM surface corrosion morphology: (a) untreated sample (b) nitrided sample after
 199 immersion in H₂S solution for 720h

200 As shown in Figure 4, the corrosion rate of the untreated 304 austenitic stainless
 201 steel (0.20 mm/a) is approximately 3.3 times that of the nitrided samples (0.06 mm/a).
 202 This indicates that the nitriding treatment can significantly improve the corrosion
 203 resistance of 304 stainless steel in the H₂S environment.

204

205

206

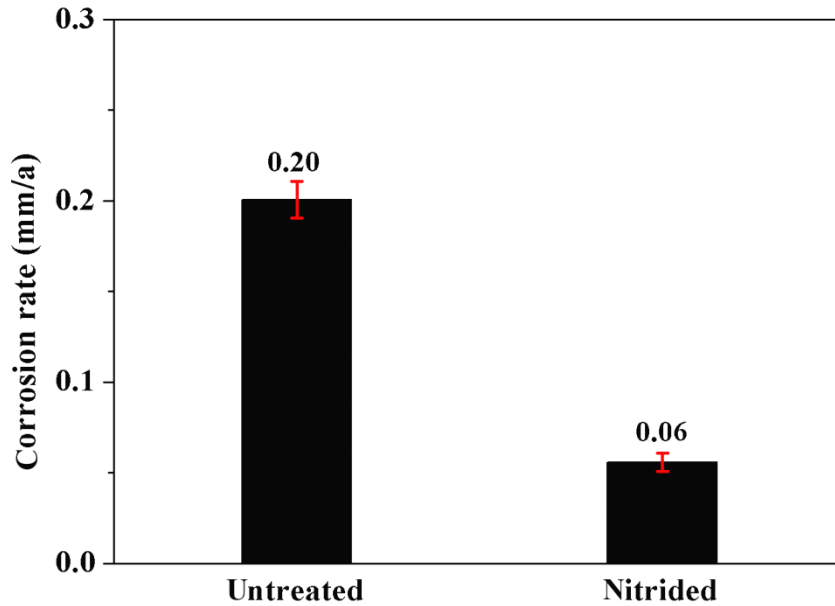


Fig.4 Corrosion rate after H₂S corrosion for 720h

207

208

209

210 The ionization of H₂S in the solution produced a large amount of H⁺, which led to
 211 a significant decrease in the pH of the solution. The ionization reaction can be
 212 described as follows: H₂S = H⁺ + HS⁻ ; 2HS⁻ = 2H⁺ + S²⁻. The ionized H⁺ is a strong
 213 depolarizer that can easily take away electrons from the metal and promote the
 214 dissolution reaction of the anode steel to cause metal corrosion. The process of
 215 electrochemically etching the cathode and the anode by H₂S is as follows:

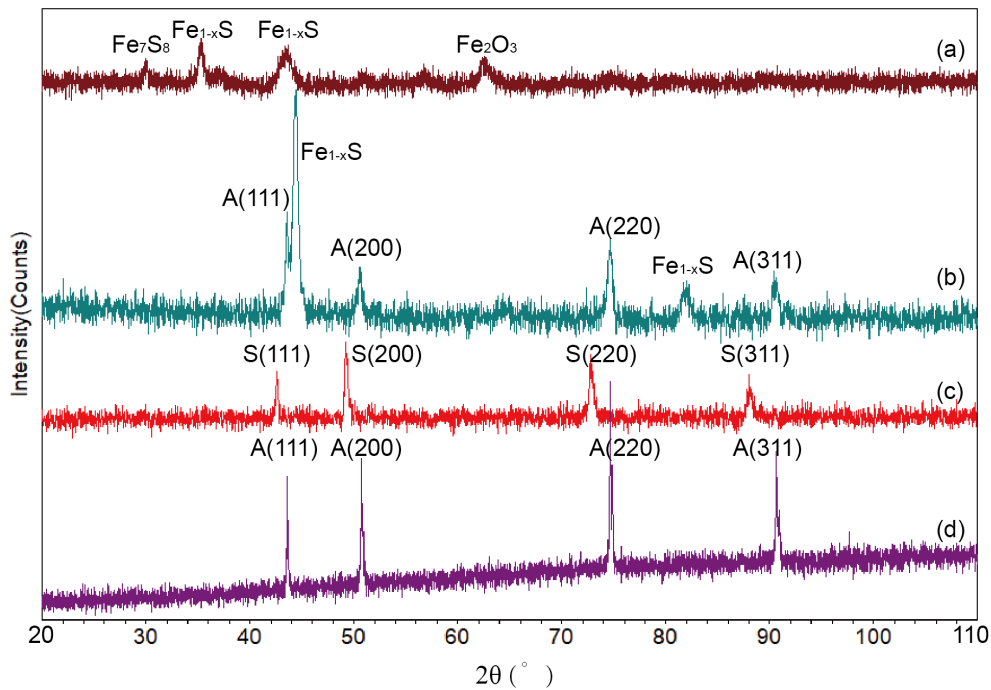
216 Cathode: Fe - 2 e⁻ → Fe²⁺;

217 Anode: 2H⁺ + 2e⁻ → 2H → H₂ ↑.

218 The anode corrosion product is: Fe²⁺ + S²⁻ = FeS↓. Therefore, after the steel is
 219 corroded by H₂S, the final product of the anode is FeS. The product usually has a
 220 defective structure with poor adhesion to the surface of steel. Hence, it can be easily
 221 detached and oxidized, and has a more positive potential. The corrosion product then
 222 acts as a cathode and the matrix to form an active microbattery and continues the
 223 corrosion of the steel. The process repeated itself and the layer eventually cracked.

224

225 3.3 XRD analysis



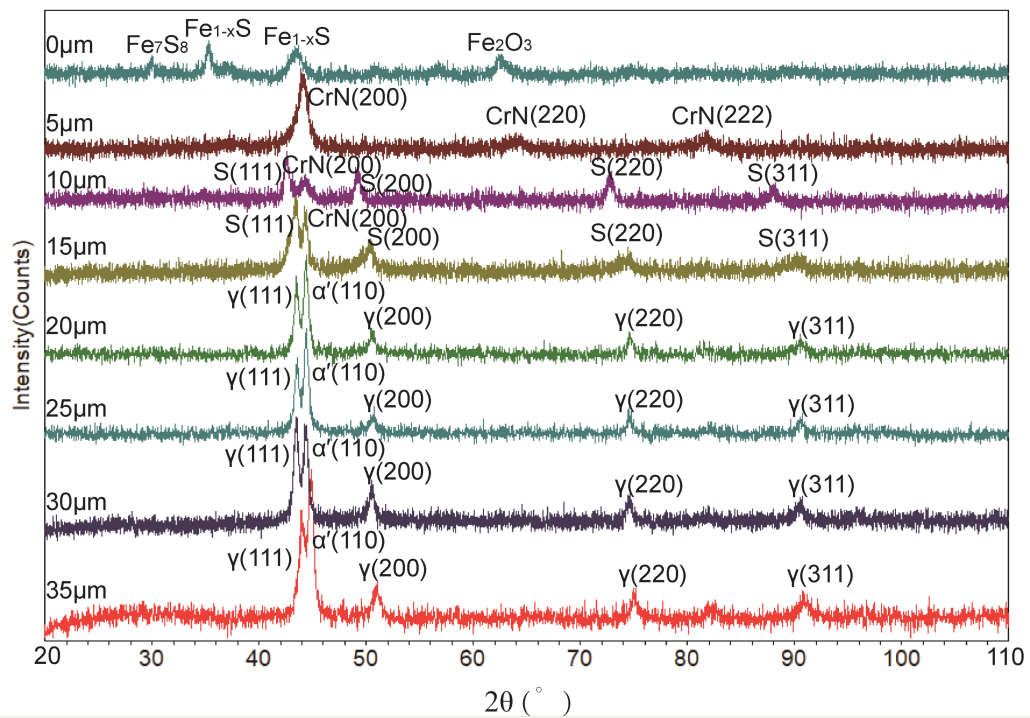
226

227

Fig.5 XRD patterns for different samples: (a) nitrided sample after corrosion test, (b) untreated sample after corrosion test, (c) as-nitrided sample and (d) untreated sample before corrosion test

228

229



230

231

Fig. 6 XRD patterns as a function of the depth below the original nitrided surface (after mechanical material removal).

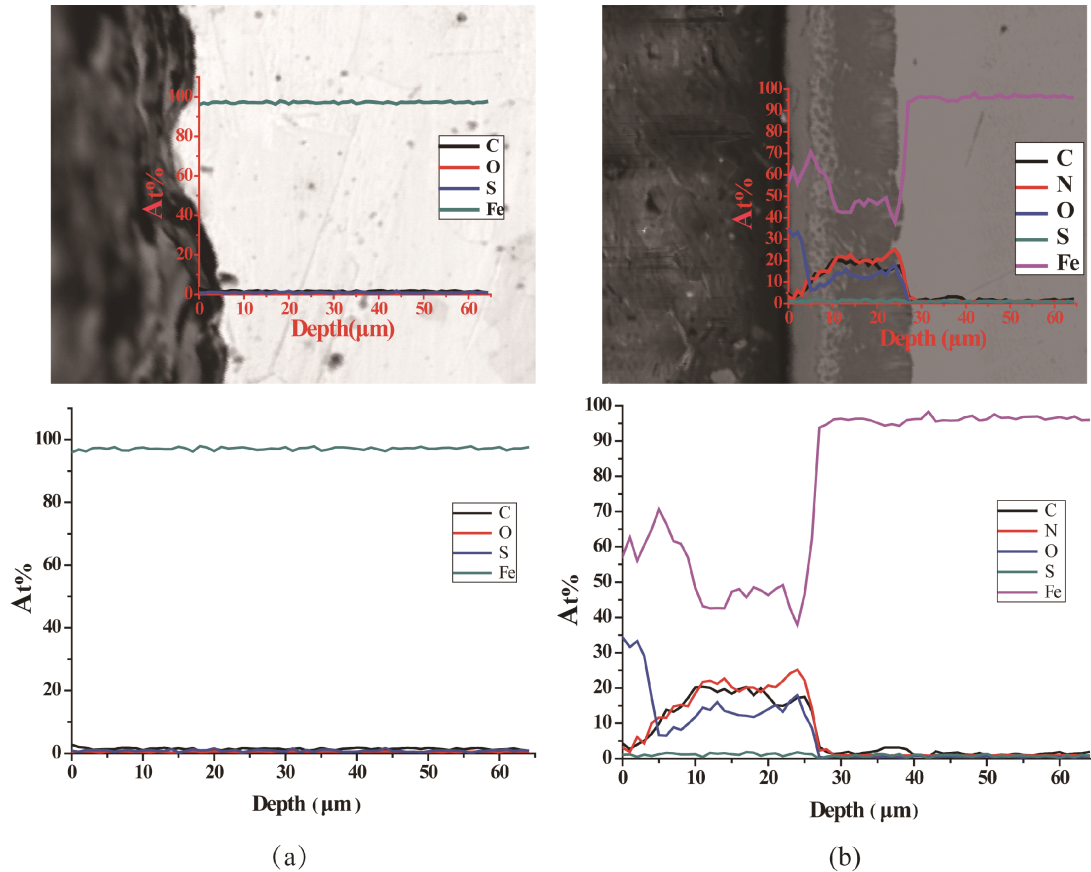
232

233 Untreated and nitrided samples were characterized by XRD to identify the
234 phases produced as a consequence of H₂S corrosion process; the diffraction patterns
235 of the samples are shown in Figure 5. It can be seen from Figure 5 that the untreated
236 sample shows typical peaks for austenite (Fig.5(d)); the nitrided sample clearly shows
237 S1(111)、S2(200)、S3(220) and S4(311) peaks. This indicates that the S-phase layer
238 has been successfully produced during nitriding. The N or C atoms dissolved in
239 austenite caused the expansion of the original face-centered cubic lattice of austenite
240 (i.e. expanded austenite) and the left-shift of these peaks.^[24] As shown in Figure 5(b),
241 the corrosion product formed on the untreated sample is Fe_{1-x}S, which shows two
242 peaks, one near γ (111) and the other between γ (200) and γ (311). Clear austenite
243 characteristic peaks can still be observed on the XRD diffraction pattern of the
244 untreated sample after H₂S corrosion. The corrosion products of the nitrided samples
245 were mainly Fe₇S₈, Fe_{1-x}S, and Fe₂O₃. Compared with the untreated samples, the
246 characteristic peaks of the expanded austenite could not be observed. This implies that
247 the nitrogen concentrations in the $\approx 5 \mu\text{m}$ thick layer below the specimen surface that
248 is sampled by the X-rays would be reduced during the H₂S corrosion test.

249 The XRD patterns obtained at different depths below the original surfaces are
250 shown in Figure 6. In the depth of 5 μm , the nitrided sample exhibits three main
251 diffraction peaks of CrN, which was formed as a consequence of the temperature of
252 the treatment, the chromium-rich alloy AISI 304, and the high nitrogen content. When
253 the nitrogen content gradually decreased with the depth, the intensity and the number
254 of CrN peaks reduced accordingly. Normally, when the AISI 304 stainless steel is
255 nitride at 703 K or below, the nitrided layer should be free of nitrides. However, the
256 as-cast 304 stainless steel used in this research may not be well annealed after cold
257 rolling, and a large amount of deformed martensite (α') was left in the matrix, as
258 evidenced by the clear α' peak detected from the substrate (Fig. 6). This resulted in
259 rapid nitrogen diffusion and precipitation of CrN. At the depth of 10 and 15 μm ,
260 distinct peaks of S phase and a weak CrN peak can be detected. Then, the
261 α' -martensite phase was detected from the depth 20 μm down to the substrate, which
262 is also contributed by the strain-induced martensite formed during the layer-by-layer
263 mechanical polishing process. Starting from the depth of 20 μm , as the interstitial atom
264 concentration gradually decreased, the lattice distortion also gradually decreased, and
265 it is better to call it γ -phase instead of S-phase. The content of interstitial atoms (C
266 N) continuously decreased with the depth and the diffraction angle of the γ -phase
267 gradually returned to normal values.

268 3.4 EPMA analysis

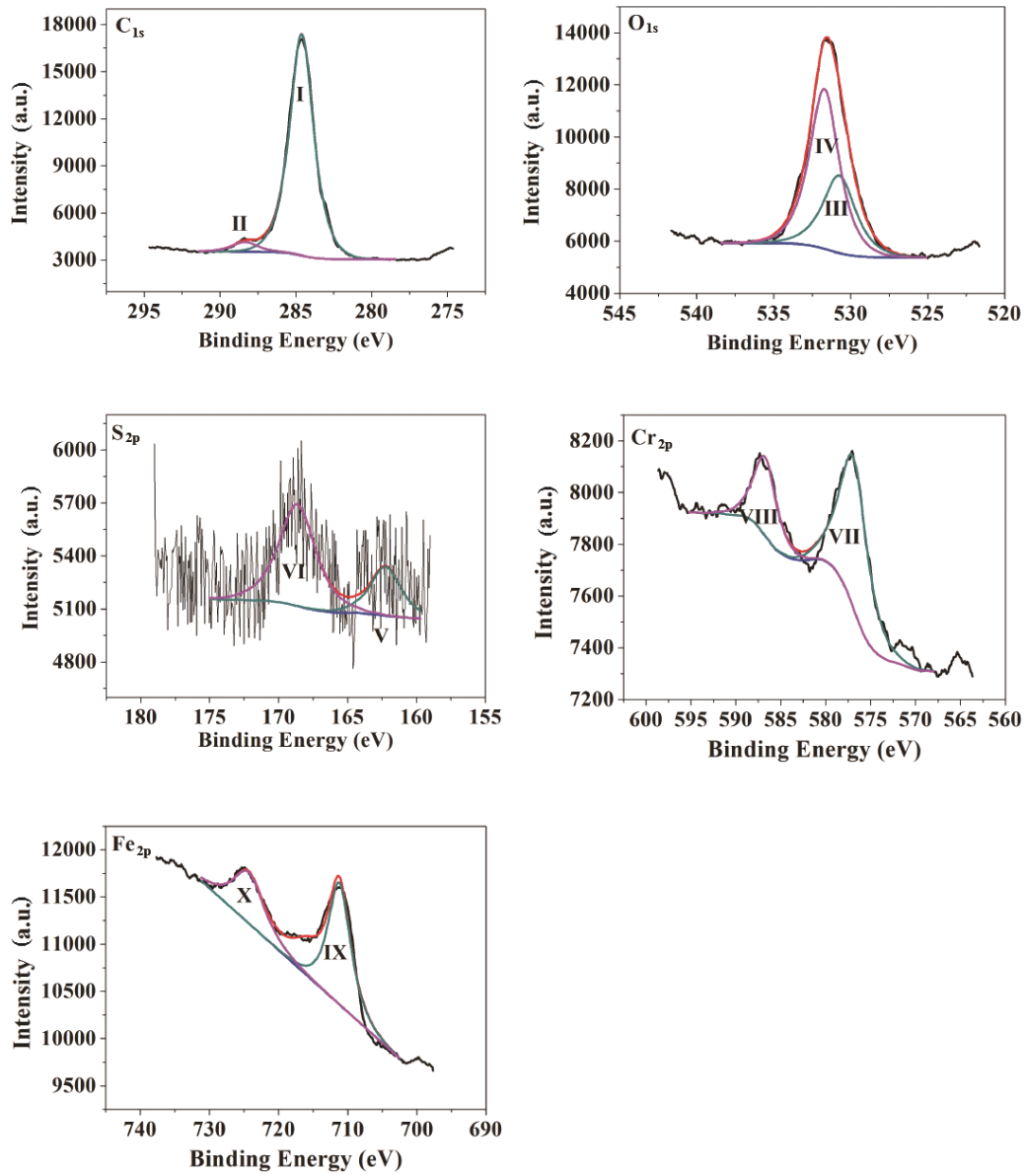
269



270
 271 **Fig.7** EPMA results of untreated (a) and nitrided samples (b) after immersion corrosion test in
 272 Solution A for 720h

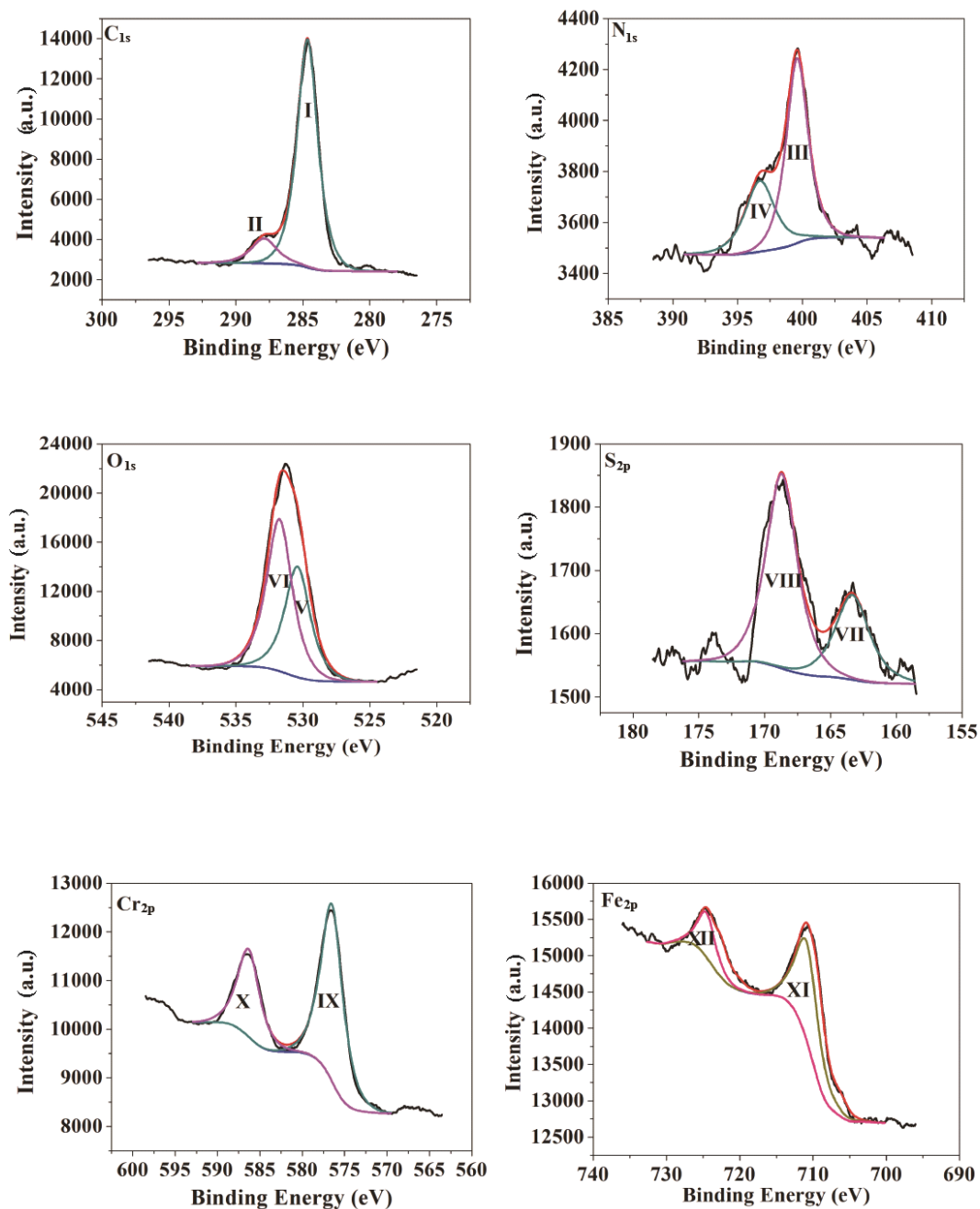
273 Figure 7 shows the EPMA results of the untreated and low temperature nitrided
 274 samples after immersion corrosion test. It can be seen by comparing Figure 7(b) with
 275 (a) that oxygen concentration increased significantly in the nitrided layer due to the
 276 oxygen atoms introduced during the nitriding process. It can be also seen that there is
 277 an oxygen plateau near the surface, which is overlapped with the grey surface layer
 278 showed in the top graph of Figure 7(b). This indicates the formation of an oxide layer
 279 during the salt bath nitriding process. The concentration of nitrogen was increased due
 280 to the formation of supersaturated austenite, which improves corrosion resistance.
 281 However, the nitrogen content decreased slightly near the surface, which may be
 282 caused by the consumption of nitrogen atoms. Combined with the results of XPS
 283 analysis, it is known that this is due to the reaction of reactive nitrogen in the nitride
 284 layer with H^+ in the H_2S solution to form NH_4^+ . For the untreated sample, the iron
 285 concentration sharply declined on the surface, which means the destruction of the
 286 passivation film, thus jeopardizing the corrosion resistance of the untreated sample
 287 leading to the appearance of a large number of corrosion pits on the surface (Fig.2(a)).
 288

289 3.5 XPS analysis



290
 291
 292
 293

Fig.8 High resolution XPS spectra of untreated samples after H₂S corrosion: C_{1s}, O_{1s}, S_{2p}, Cr_{2p}, Fe_{2p}.



294
 295
 296
 297
 298
 299
 300
 301

Fig.9 High resolution XPS spectra of nitrated samples after H₂S corrosion: C_{1s}, N_{1s}, O_{1s}, S_{2p}, Cr_{2p}, Fe_{2p}.

Table2 Binding energy and specification for the elements by XPS analysis of nitrated and untreated samples after H₂S corrosion

Element		BE(eV)	peak	at%
untreated				
C	1s	284.6	Adventitious/C, I	19.79
	1s	288.3	Adventitious, II	1.89
O	1s	530.7	Cr ₂ O ₃ , III	15.46
	1s	531.7	FeOOH, IV	28.91
S	2p	162.2	FeS ₂ , V	3.78
	2p _{3/2}	168.6	SO ₄ ²⁻ , VI	9.40
Cr	2p _{3/2}	576.8	Cr ₂ O ₃ , VII	3.90
	2p _{1/2}	586.8	Cr(OH) ₃ , VIII	1.66
Fe	2p _{3/2}	711.2	Fe ₂ O ₃ , IX	9.65
	2p _{1/2}	724.3	FeOOH, X	5.56
nitrided				
C	1s	284.6	Adventitious/C, I	45.04
	1s	288.3	Adventitious, II	6.07
N	1s	396.7	CrN, III	0.98
	1s	399.6	NH ₄ ⁺ , IV	1.89
O	1s	530.7	Cr ₂ O ₃ , V	16.78
	1s	531.7	FeOOH, VI	23.16
S	2p _{1/2}	163.5	FeS ₂ , VII	0.10
	2p _{3/2}	168.6	SO ₄ ²⁻ , VIII	0.20
Cr	2p _{3/2}	576.5	Cr ₂ O ₃ , IX	2.58
	2p _{1/2}	586.3	Cr ₂ O ₃ , X	1.27
Fe	2p _{3/2}	710.8	Fe ₂ O ₃ , XI	1.42
	2p _{1/2}	724.3	FeOOH, XII	0.51

303 Elemental contributions analyses have been performed for carbon, nitrogen,
 304 oxygen, sulfur, chromium and iron on the H₂S corrosion tested surface of untreated
 305 and as-nitrided samples and the results are reported in Figure 8 and Figure 9,
 306 respectively. The parameters and corresponding atomic contents are detailed in Table
 307 2.

308 Oxygen (O_{1s}) contribution in both untreated and nitrided sample appears as two
 309 visible although entangling peaks: one for oxides at 530.7 eV and one for hydroxides
 310 at 531.7 eV.^[25] XPS analysis results showed that the corrosion products formed on the
 311 untreated and nitrided samples were approximately the same, mainly Fe₂O₃, FeOOH.
 312 The corrosion products detected by XRD are mainly sulfides, whilst the corrosion
 313 products detected by XPS are mainly oxides. This is because the detection depth of
 314 the two techniques is different: the detection depth of XRD is usually in the micron
 315 range, but the XPS detection is in the nanoscale. Therefore, it can be considered that
 316 the corrosion product is layered with the oxide content enriched in the outer layer and
 317 the sulfide content in the inner layer.

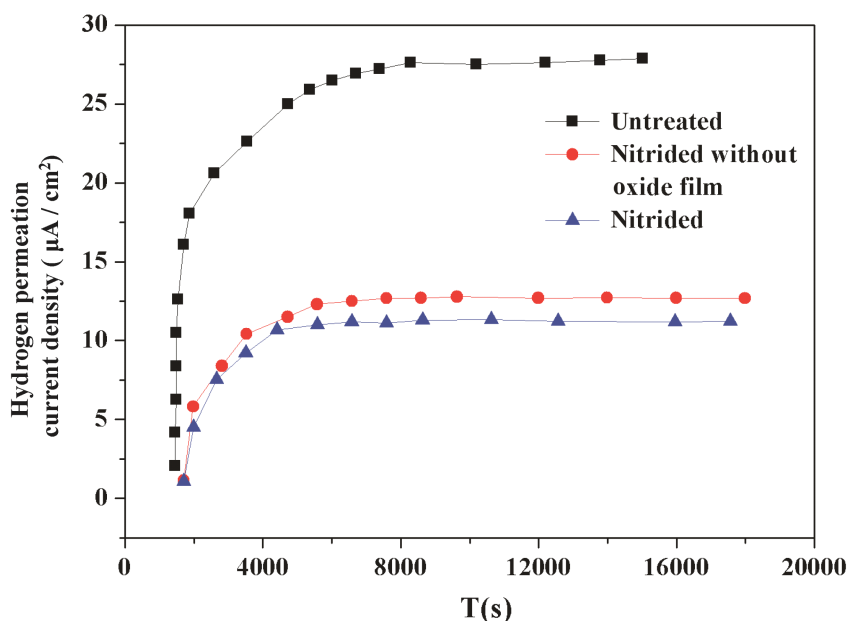
318 The characteristic peaks of Cr in nitrided and untreated samples are mainly Cr₂O₃
 319 and a small amount of Cr(OH)₃. Chromium accumulated in the corrosion product film
 320 to form a stable amorphous Cr (OH)₃, which makes the film more stable. At the same

321 time, the corrosion product film mainly containing $\text{Cr}(\text{OH})_3$ has a certain cation
322 selective permeability. It can effectively prevent the anion from penetrating the
323 corrosion product film to the metal surface and reduce the corrosion rate of the
324 material.^[26] Since $\text{Cr}(\text{OH})_3$ is amorphous,^[27] it does not be detected by XRD.

325 For the S_{2p} fit spectrum, 162.2 eV and 163.5 eV can be considered as the peak of
326 $\text{FeS}_{1.15}$, which is consistent with the previous analysis. 168.6 eV can be considered as
327 a characteristic peak of sulfate, such as FeSO_4 , $\text{Fe}_2(\text{SO}_4)_3$, etc. The presence of
328 sulfates was not expected to be formed in H_2S electrolyte due to the absence of
329 oxygen in solution, which could be the consequence of sulfide oxidation during the air
330 exposition between the end of aging in the H_2S solution and the XPS measurements.
331 For the nitrated samples, 396.7 eV can be regarded as a characteristic peak of CrN in
332 N_{1s} fit spectrum. 399.6 eV can be regarded as a characteristic peak of NH_4^+ , indicating
333 that the active nitrogen of the nitrated layer reacts with H^+ in the H_2S solution,
334 consumes H^+ , lowers the pH and protects the metal. The experimental result is
335 consistent with our previous finding.^[28]

336 It can be found from Table 2 that after the H_2S corrosion, the S content (13.27 at%)
337 and Fe content (12.51 at%) of the untreated sample are significantly larger than that of
338 the nitrated sample (0.3 at% S and 1.93 at% Fe). On the one hand, it is shown that
339 nitrating can prevent the formation of corrosion products on the surface of the sample,
340 and on the other hand, it also indicates that the corrosion product is difficult to deposit
341 on the surface of the sample. The literature indicates that under certain conditions, the
342 corrosion product film has no protective effect on the substrate and may even lead to
343 an increase in the corrosion rate.^[29-31] Since the nitrated layer reduced the production
344 of corrosion products, further corrosion of the sample can be prevented.

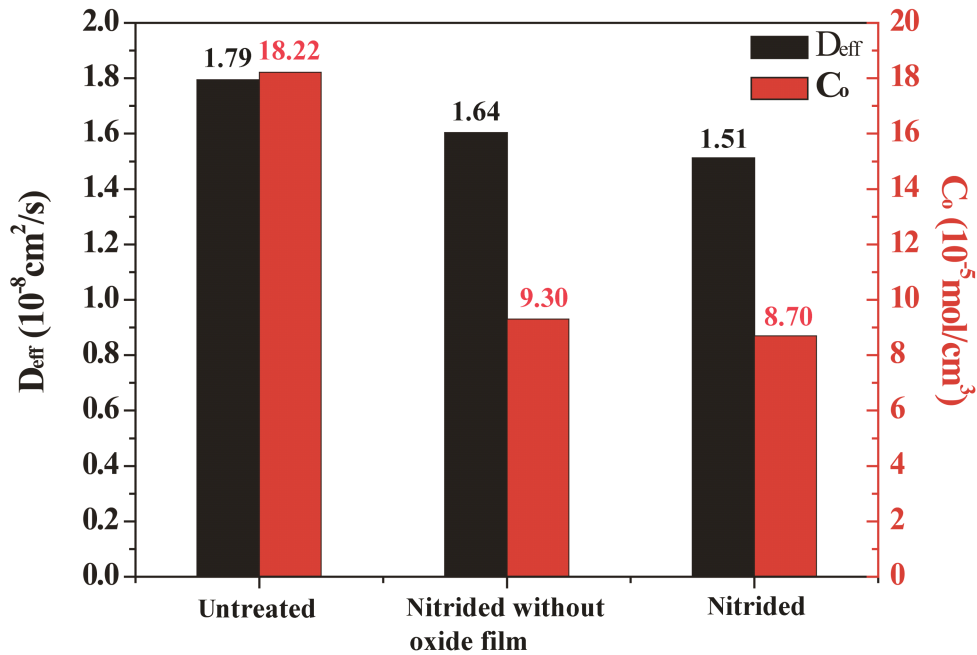
345 3.6 Hydrogen permeation analysis



346

347
348

Fig.10 Hydrogen permeation current density curves of samples under different conditions.



349
350
351

Fig. 11 Diffusion coefficients and hydrogen atom concentrations curve of the sample under different conditions.

352
353
354
355
356
357
358
359
360
361
362
363
364
365
366
367
368
369
370
371
372
373

Hydrogen permeation occurring on the surface of pipe steel is one of the main risks of steel failure, and the intensity of which can be reflected in the hydrogen permeation current. [32] Zhang et al. investigated the effect of the cathodic current density (i) on the permeation of hydrogen through X80 pipeline steels using an electrochemical permeation technique and they provided an equation to describe the relationship between concentration of hydrogen (C_0) and cathodic current density (i), this equation indicated that C_0 increased with i . [33] The hydrogen permeation current density curves of different samples are shown in Figure 10. It can be seen that the anodic steady-state current density of untreated samples is significantly greater than that of as-nitrided samples and nitrided & oxide film removed samples. In addition, the untreated sample took a longer period to reach the steady state anode current density than the as-nitrided samples and the nitrided & oxide film removed samples. Figure 11 shows the hydrogen diffusion coefficient D_{eff} and hydrogen concentration C_0 for different materials states. The results show that the hydrogen concentration in the untreated sample ($18.22 \times 10^{-5} \text{ mol}/\text{cm}^2$) is significantly higher than that of the as-nitrided sample ($9.30 \times 10^{-5} \text{ mol}/\text{cm}^2$) and the nitrided & oxide film removed samples ($8.70 \times 10^{-5} \text{ mol}/\text{cm}^2$). The reason for this may be that the nitrided layer could trap a large amount of hydrogen, thus resulting in a substantial reduction of hydrogen absorption by the substrate. [34] The hydrogen diffusion coefficient ($1.79 \times 10^{-8} \text{ cm}^2/\text{s}$) of the untreated sample is larger than that of the as-nitrided sample ($1.64 \times 10^{-8} \text{ cm}^2/\text{s}$) and nitride & oxide film removed sample ($1.51 \times 10^{-8} \text{ cm}^2/\text{s}$), indicating the nitrided layer and oxide layer can reduce the diffusion coefficient of hydrogen.

374 4. Discussion

375 4.1 The effect of the nitrated layer on hydrogen permeation

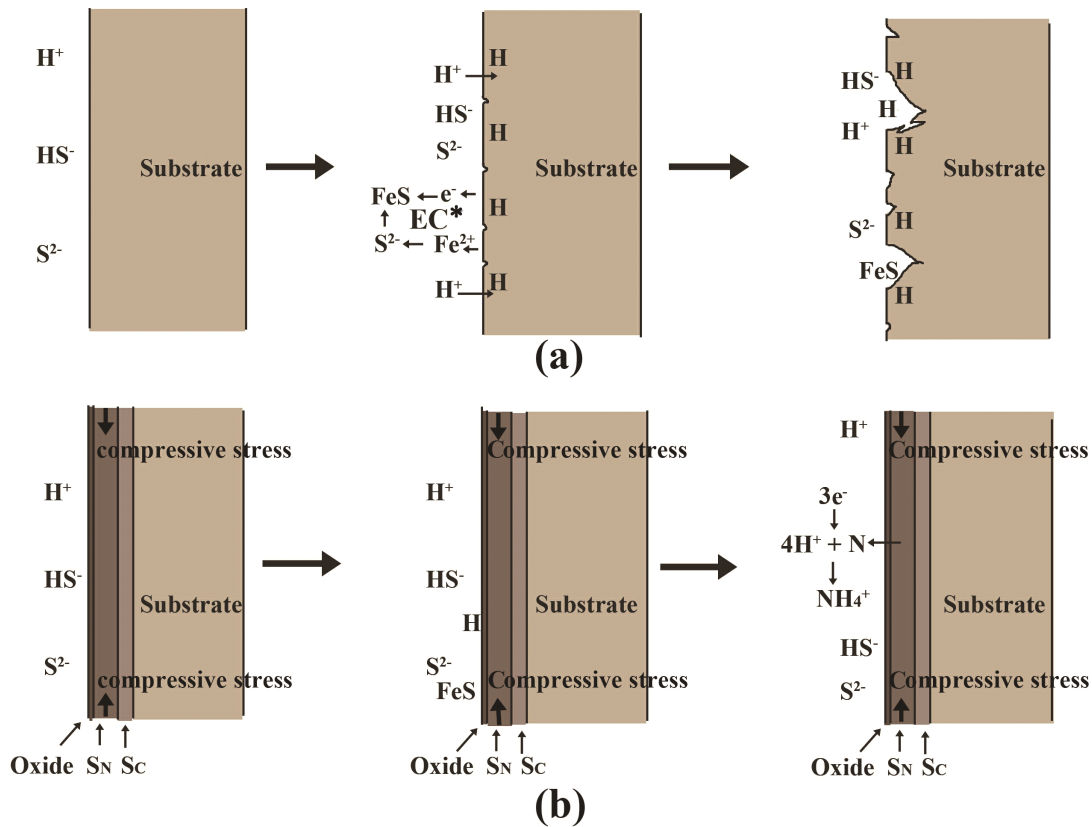
376 When the sample is soaked in the H₂S containing solution for a long time, H₂S
377 reacts with the surface of the steel to produce hydrogen, which then enters the steel
378 matrix, building up pressure that leads to embrittlement.^[35] Research has shown that
379 supersaturated interstitials cause large lattice expansion while the non-nitrated bulk
380 material constrains this expansion, causing the nitrated layer to have very high
381 residual compressive stresses.^[36] Therefore, the residual compressive stress helps to
382 relieve the tensile stress caused by the H atoms, thus preventing hydrogen
383 embrittlement. However, when the sample is in a stress corrosion environment and the
384 applied tensile stress increases to a certain extent, the residual compressive stress of
385 the S-phase layer may be cancelled out and hydrogen-induced cracking can occur.^[28]
386 From the results of electrochemical hydrogen permeation experiment (Fig.10 and Fig
387 11), it can be seen that both the nitrated layer and the oxide layer help reduce the
388 diffusion coefficient of hydrogen and the amount of hydrogen atoms entering the
389 material, thus shorting the time required for the anode current to reach equilibrium.
390 The possible reason is that the nitrating layer can trap a large amount of hydrogen,
391 resulting in a substantial reduction of hydrogen absorption by the substrate,^[34] as
392 shown in Figure 11.

393 Research has shown that electrochemical H-charging of pulsed plasma nitrated
394 austenite resulted in a softening effect within the compound layer (S-phase).^[37] The
395 hydrogen in the lattice acts as a solution softening agent and the softening or
396 hardening effect of the hydrogen is dependent on the nitrogen concentration and the
397 dislocation density of the material. As can be seen from Figure 7, the nitrogen
398 concentration exceeds 20 at%. When hydrogen ions enter the nitrated layer with a
399 very high interstitial atom content, it softens and prevents hydrogen embrittlement.

400 4.2 The effect of the nitrating on H₂S corrosion

401 Figure 12 schematically shows the H₂S corrosion model for untreated and nitrated
402 specimens. As shown in Figure 12(a), acidic H₂S solution hydrolyzes H⁺, HS⁻, S²⁻,
403 which reacts on the surface of the steel to produce Fe²⁺. When acidic chemical
404 corrosion occurs, the inherent protective film on the pipe surface is destroyed, causing
405 the corrosive medium to enter the interior of the metal crystal and generating
406 electrochemical corrosion. Electrochemical corrosion forms an etched primary cell.
407 The anode process is a dissolution reaction of the metal, and the cathode undergoes a
408 hydrogen depolarization reaction. Anodic sulphide corrosion products deposit on the
409 metal surface, which is poorly protective and in fact promotes the corrosion of the
410 stainless steel substrate. Monnot et al. highlighted the role of corrosion products on
411 the failure mechanism of martensitic stainless steels in sour media.^[38] Corrosion
412 product formed under this condition has a high level of porosity and is prone to
413 spalling due to cracks and defects throughout the amorphous structure. In fact, H₂S
414 diffuses on the surface of the etching film and penetrates along the porous structure,
415 and reacts at the metal/film interface. The metal sulphide is formed to release the
416 hydrogen previously bound to the sulfur that can be absorbed by the alloy. Corrosion

417 product films therefore correspond to a rich hydrogen reservoir near the metal surface
 418 that can trigger and maintain hydrogen uptake. The data in Table 2 show that nitriding
 419 treatment can effectively reduce the generation of corrosion products, thereby
 420 alleviating hydrogen embrittlement and corrosion.
 421



Note: * stands for electrochemical corrosion.

422

Fig.12 H₂S corrosion model of (a) untreated sample and (b) nitrided sample

423

424

425

426

427

428

429

430

431

432

433

434

435

436

437

438

The oxide layer can effectively prevent the corrosion of acidic H₂S as schematically shown in Figure 12(b). Granda—Gutiérrez et al. found that post-oxidation following nitriding treatment increased the time to SSC rupture of stainless steel by a factor of 10 because the dense oxide film on the surface after the treatment significantly improved the resistance to H₂S corrosion cracking of the stainless steel.^[39] This is partially because the nitride layer reduced the generation of corrosion products (Table 2) and partially because it also prevented hydrogen atoms (Fig.11) from entering the substrate, thereby preventing electrochemical corrosion.

Nitrogen can effectively improve the local corrosion resistance of stainless steel,^[40] and some hypotheses have been put forward to explain this behavior: (1) high concentration of nitrogen atoms on the surface of stainless steel stabilizes passive film and inhibits dissolution;^[41-43] (2) formation of NO₃⁻ (nitrate) ions leads to increased pitting resistance;^[44] (3) stabilization effect of nitrogen on austenite.^[45] For the nitrided samples produced in this research, there are a large amount of active nitrogen

439 atoms in the surface of the sample after low temperature nitriding due to the high
440 level of chromium, nickel, molybdenum in the matrix material . The fitted spectra of
441 N1s from the nitriding samples after being soaked in H₂S solution are shown in Figure
442 9. H⁺ reacts with the nitrogen atom via the reaction: $N + 4H^+ = NH_4^+$. This consumed
443 the H⁺ in the solution prevented the pH of the metal surface from decreasing, and
444 thereby increased the corrosion resistance of the alloy, which is consistent with the
445 EPMA results in Figure7. At the same time, the active nitrogen atoms can accelerate
446 the formation of passivation film and affect the repassivation kinetics, so that the
447 passivation film can grow stably and increase the density of the passivation film.^[46]

448 **5. Conclusions**

449 Low-temperature liquid nitrided samples have better corrosion resistance than
450 untreated samples in H₂S environment. The corrosion rate of the untreated sample is
451 about 3.6 times that of the nitriding sample; clear corrosion pits can be observed on
452 the surface of the untreated sample, while the treated sample surface remains almost
453 intact. Due to the presence of oxide layers, despite precipitation of CrN in the
454 nitriding layer, the corrosion resistance of the sample after the nitriding treatment in
455 the H₂S environment is still significantly improved by the treatment.

456 The corrosion products are mainly consisted of oxides, hydroxides, and sulfates.
457 The nitrided layer reduces the production of corrosion products; further corrosion of
458 the sample is thus prevented. Both oxide layer and nitrided layer can reduce the
459 diffusion coefficient of hydrogen and the amount of hydrogen atoms entering the
460 material, which is beneficial to improving the resistance to hydrogen embrittlement.
461 Nitriding layer is supersaturated with active nitrogen atoms, which combine with H⁺
462 to avoid surface pH reduction, thus decelerating H₂S corrosion.

463 **Acknowledgement**

464 The authors are very grateful to the grants provided by National Natural Science
465 Foundation of China (No. 51471112 and 51611130204), Science and Technology
466 Planning Project of Sichuan (No.2016GZ0173) and the Newton Mobility Grant from
467 Royal Society, UK (IE151027).

468

469 **References**

- 470 1. K. Komai, *Int. J. Fatigue.*, 1998, vol. 20, pp. 145-154.
- 471 2. M. L. Medvedeva and V. V. Gur'Yanov, *Prot. Met.*, 2002, vol. 38, pp. 284-288.
- 472 3. D. W. Shoesmith, P. Taylor, M. G. Bailey and D. G. Owen, *Cheminform*, 1980, vol. 11, pp.
473 1007-1015.
- 474 4. H. Yang, J. Chen, C. Cao, D. Cao and X. Jiang, *J. Chin. Soc. Corros. Rrot.*, 2001, vol. 21, pp.
475 321-327.
- 476 5. H. Wang, P. Zhou, S. Huang, C. Yu, *Int. J. Electrochem. Sci.*, 2016, vol. 11, pp. 1293-1309.
- 477 6. J. Fliethmann, H. Schlerkmann and W. Schwenk, *Corros. Sci.*, 1992, vol. 24, p. 746.
- 478 7. J. Ding, Z. Lei, M. Lu, J. Xue and Z. Wen, *J. Mater. Sci. Technol.*, 2013, vol. 48, pp. 3708-3715.
- 479 8. S. K. Putatunda, *Mat. Sci. Eng. R.*, 1986, vol. 82, pp. L7-L11.

- 480 9. W.T. Tsai and S.L. Chou, *Corros. Sci.*, 2000, vol. 42, pp. 1741-1762.
- 481 10. L. F. Li, Z. Q. Huang and X. M. Liu, *Adv. Mater.*, 2012, vol. 485, pp. 393-396.
- 482 11. A. Heuer and S. Collins, *Metall. Mater. Trans. A.*, 2009, vol. 40, pp. 1767-1767.
- 483 12. G. M. Michal, F. Ernst, H. Kahn, Y. Cao, F. Oba, N. Agarwal and A. H. Heuer, *Acta. Mater.*, 2006,
- 484 vol. 54, pp. 1597-1606.
- 485 13. X. Y. Li and H. Dong, *Met. Sci. J.*, 2003, vol. 19, pp. 1427-1434.
- 486 14. S.J.B.Kurza, S.R.Mekaa, N.Schellb, W.Eckerc, J.Keckesd, E.J.Mittemeijerae, *Acta. Mater.*, 2015,
- 487 vol. 87,pp.100-110.
- 488 15. L. Zhang, C. Ren, Q. Yu, J. Zhang, S. Sun, Q. Ren, Y. Lian, X. Chen and W. Gao, *Surf. Coat.*
- 489 *Technol.*, 2017, vol. 315, pp. 95-104.
- 490 16. J. Wang, Y. Lin, J. Yan, D. Zeng, R. Huang and Z. Hu, *Isij Int.*,2012, vol. 52, pp. 1118-1123.
- 491 17. M. A. V. Devanathan, Z. Stachurski, *Proc. Royal. Soc. Lond*, 1962, vol. 270(1340), pp. 90-102
- 492 18. S. Shen, X. Li, P. Zhang, Y. Nan, G. Yang: *Mater. Sci. Eng. A* 2017, vol. 703, pp: 413-421
- 493 19. H. Hu, K. Li, W. Wu, G.X.Chen, W.J.Chen: *J. Xi'an Jiaotong Univ.* 2016, vol. 50(07). 89-95.
- 494 20. C. Zhou, S. Zheng, C. Chen and G. Lu, *Corros. Sci.*, 2013, vol. 67, pp. 184-192.
- 495 21. R.A. Carneiro, R. C. Ratnapuli and V. D. F. C. Lins, *Mat. Sci. Eng. A.*, 2003, vol. 357, pp.
- 496 104-110.
- 497 22. C. F. Dong, Z. Y. Liu, X. G. Li and Y. F. Cheng, *Int. J. Hydrogen. Energ.*, 2009, vol. 34, pp.
- 498 9879-9884.
- 499 23. M. Tsujikawa, N. Yamauchi, N. Ueda, T. Sone and Y. Hirose, *Surf. Coat. Technol.*, 2005, vol. 193,
- 500 pp. 309-313.
- 501 24. W. Shi, X. Y. Li and H. Dong, *Wear.*, 2001, vol. 250, pp. 544-552.
- 502 25. M. Mantel and J. P. Wightman, *Surf. Interface. Anal.*, 1994, vol. 21, pp. 595-605.
- 503 26. C. F. Chen, W. F. Chang, Z. H. Zhang, M. X. Lu and D. B. Sun, *Corrosion -Houston Tx-* 2005, vol.
- 504 61, pp. 594-601.
- 505 27. J. Sun, C. Sun, X. Lin, X. Cheng and H. Liu, *Materials.*, 2016, vol. 9, p. 200.
- 506 28. X. Zhang, J. Wang, H. Fan, J. Yan, L. Duan, T. Gu, G. Xian, L. Sun and D. Wang, *Metall. Mater.*
- 507 *Trans. A.*,2018, vol. 49, pp. 356-367.
- 508 29. D. R Morris, L. P Sampaleanu and D. N Veysey, *J. Electrochem. Soc.*, 1980, vol. 127, pp.
- 509 1228-1235.
- 510 30. F. H. Meyer, O. L. Riggs, R. L. Mcglasson and J. D. Sudbury, *Corrosion -Houston Tx-* 1958, vol.
- 511 14, pp. 109-115.
- 512 31. J. S. Smith and J. D. A. Miller, *Brit. Corros. J.*, 2013, vol. 10, pp. 136-143.
- 513 32. C. Zhou, X. Chen, Z. Wang, S. Zheng, X. Li, L. Zhang, *Corros. Sci.* 2014, vol. 89, pp: 30-37
- 514 33. L. Zhang, W. Cao, K. Lu, Z. Wang, Y. Xing, *Int. J. Hydrogen Ener*, 2017, vol. 42(5), pp:
- 515 3389-3398.
- 516 34. T. Zakroczymski, J. Flis, N. Lukomski and J. Mankowski, *Acta.Mater.*, 2001, vol. 49, pp.
- 517 1929-1938.
- 518 35. Z. Y. Liu, C. F. Dong, X. G. Li, Q. Zhi and Y. F. Cheng, *J. Mater. Sci.*, 2009, vol. 44, pp.
- 519 4228-4234.
- 520 36. A. H. Heuer, F. Ernst, H. Kahn, A. Avishai, G. M. Michal, D. J. Pitchure and R. E. Ricker, *Scripta*
- 521 *Mater.*, 2007, vol. 56, pp. 1067-1070.
- 522 37. M. Asgari, A. Barnoush, R. Johnsen and R. Hoel, *Corros. Sci.*, 2012, vol. 62, pp. 51-60.
- 523 38. M. Monnot, R.P. Nogueira, V. Roche, G. Berthomé, E. Chauveau, R. Estevez, M. Mantel, *Appl.*

- 524 *Surf. Sci.*, 2017, 394:132-141.
- 525 39. E. E. Granda-Gutiérrez, J. C. Díaz-Guillén, J. A. Díaz-Guillén, M. A. González, F.
526 García-Vázquez and R. Muñoz, *J. Mater. Eng. Perform.*, 2014, vol. 23, pp. 4148-4153.
- 527 40. P. G. Esteban, L. Bolzoni, E. M. Ruiznavas and E. Gordo, *Power Metall.*, 2011, vol. volume 54,
528 pp. 242-252(11).
- 529 41. Y. C. Lu, R. Bandy, C. R. Clayton and R. C. Newman, *Cheminform.*, 1983, vol. 14, pp.
530 1774-1776.
- 531 42. H. Baba, T. Kodama and Y. Katada, *Corros. Sci.*, 2002, vol. 44, pp. 2393-2407.
- 532 43. C.O. A. Olsson, *Corros. Sci.*, 1995, vol. 37, pp. 467-479.
- 533 44. H. P. Leckie, *J.electrochem. soc.*, 1966, vol. 113, pp. 1262-1267.
- 534 45. J. W. Simmons, *Mat. Sci. Eng. A.*, 1996, vol. 207, pp. 159-169.
- 535 46. P. R. Levey and A. R. V.Bennekom, *Corrosion.*, 1995, vol. 51, pp. 911-921.

536 **Fig.1** A typical cross sectional SEM image of nitrided sample

537

538 **Fig.2** Cross-sectional optical micrographs (OM): (a) untreated sample (b) nitrided
539 sample after immersion in H₂S solution for 720h

540

541 **Fig.3** SEM surface corrosion morphology: (a) untreated sample (b) nitrided sample
542 after immersion in H₂S solution for 720h

Fig.4 Corrosion rate after H₂S corrosion for 720h

543

544 **Fig.5** XRD patterns for different samples: (a) nitrided sample after corrosion test, (b)
545 untreated sample after corrosion test, (c) as-nitrided sample and (d) untreated sample
546 before corrosion test

547 **Fig. 6** XRD patterns as a function of the depth below the original nitrided surface
548 (after mechanical material removal).

549 **Fig.7** EPMA results of untreated (a) and nitrided samples (b) after immersion
550 corrosion test in Solution A for 720h

Fig.8 High resolution XPS spectra of untreated samples after H₂S corrosion: C1s, O1s,
S2p, Cr2p, Fe2p.

Fig.9 High resolution XPS spectra of nitrided samples after H₂S corrosion: C1s, N1s,
O1s, S2p , Cr2p , Fe2p .

551 **Fig.10** Hydrogen permeation current density curves of samples under different
552 conditions.

Fig.11 Diffusion coefficients and hydrogen atom concentrations curve of the
sample under different conditions.

Fig.12 H₂S corrosion model of (a) untreated sample and (b) nitrided sample

Table 1 Chemical composition of AISI 304 stainless steel (mass%)

Table 2 Binding energy and specification for the elements by XPS analysis of nitrided
and untreated samples after H₂S corrosion